Rock Mech. Rock Engng. (2002) 35 (3), 141–160
DOI 10.1007/s00603-001-0019-4

Rock Mechanics and Rock Engineering
Printed in Austria

Effect of Elastic Anisotropy on Tunnel Wall Displacements Behind a Tunnel Face

By

F. Tonon and **B. Amadei**

Department of Civil Engineering, University of Colorado, Boulder, U.S.A.

Received June 23, 2000; accepted September 18, 2001
Published online August 2, 2002 © Springer-Verlag 2002

Summary

The effect of elastic anisotropy (transverse isotropy) on the convergence behind a tunnel face is investigated by means of a parametric study. The applicability of existing expressions for evaluating the convergence behind a tunnel face is also addressed. Two cases are distinguished, according to whether the plane of transverse isotropy strikes parallel to the tunnel axis or not. It is found that the existing expressions (valid for isotropic rock masses under a uniform state of stress) are applicable only when the plane of transverse isotropy strikes parallel to the tunnel axis. When the plane of transverse isotropy does not strike parallel to the tunnel axis, three-dimensional analyses are necessary.

1. Introduction

The determination of tunnel wall convergence that occurs before installation of reinforcement and/or lining is of fundamental importance in two-dimensional models of underground excavations (e.g. Mammino and Tonon, 1997). This is clearly shown in Fig. 1, which illustrates the deformed shape of a circular tunnel in an isotropic medium under a uniform state of stress. The displacement magnitude of the tunnel walls is an increasing function of the distance d to the tunnel face.

The determination of this function has been vigorously addressed in the literature starting from the early 1980's (see Mammino and Tonon, 1997 for a thorough review). In general, isotropic rock masses (both elastic and elastoplastic) under a uniform state of stress were considered, and parametric FEM simulations were conducted. Apparently, the effect of elastic anisotropy on the convergence behind a tunnel face has not been thoroughly addressed in the published literature.

In this paper, a parametric study is presented for the case of a transversely isotropic rock mass. The Boundary Element method is utilized to carry out the calculations. Two cases are distinguished, according to whether the plane of transverse

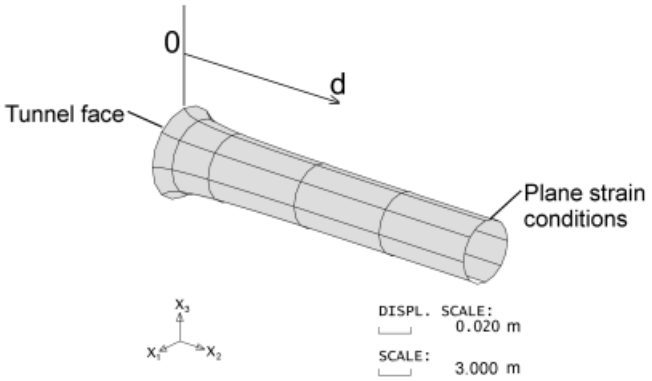

Fig. 1. Deformed shape of a tunnel excavated in an isotropic medium under a uniform *in situ* state of stress

isotropy strikes parallel to the tunnel axis or not. The stiffness of the reinforcement/lining is not taken into account, i.e. an unlined tunnel is considered.

2. Tunnel Convergence for Isotropic Rock Masses Under a Uniform State of Stress

Expressions for convergence of a tunnel excavated in an isotropic medium under a uniform state of stress have been proposed in the literature. Such expressions can be divided into two types:

1) The convergence is only a function of the distance d to the tunnel face.
2) The convergence is considered as a function of the distance d to the tunnel face and of the relative stiffness of the lining to the rock mass.

Let E and v be the Young's modulus and the Poisson's ratio of the rock mass, respectively, d be the distance to the tunnel face, and R be the tunnel radius. According to the first approach, for an elastic isotropic rock mass under a uniform *in situ* state of stress p_0, Panet and Guenot (1982) derived the following expression based on the results of three-dimensional Finite Element models:

$$|\mathbf{v}| = |\mathbf{v}_f| \cdot \left\{ 0.28 + 0.72 \cdot \left[1 - \left(\frac{1}{1 + \frac{d}{0.84R}} \right)^2 \right] \right\}, \tag{1}$$

where:

$|\mathbf{v}|$ = amount of tunnel wall displacement (in this case mainly radial).

$|\mathbf{v}_f| = \dfrac{1+v}{E} \cdot p_0 \cdot R$ = convergence occurring far away from the tunnel face (plane strain condition) for zero internal pressure applied to the tunnel wall.

Similarly, again on the basis of Finite Element calculations, Corbetta et al. (1991) proposed:

$$|\mathbf{v}| = |\mathbf{v}_f| \cdot \{0.29 + 0.71 \cdot [1 - e^{-1.5 \cdot (d/R)^{0.7}}]\}. \quad (2)$$

It can be noticed that, according to Eqs. (1) and (2), 30% of the maximum convergence $|\mathbf{v}_f|$ already occurs at the tunnel face ($d = 0$). Expressions (1) and (2) have been modified by Panet and Guenot (1982), and Corbetta et al. (1991), respectively, for elasto-plastic rock masses.

Different formulations have been proposed by Bernaud and Rousset (1992, 1996), and Nguyen-Minh and Guo (1993, 1996) in order to take into account the presence of the reinforcement/lining already installed.

3. Boundary Element Model

Because we are exclusively interested in the elastic deformation of the tunnel wall, a Boundary Element model is very efficient. Program BEFE Version 6.4 (Beer, 1999) was used for carrying out the analyses. This version of the program includes the subroutines for Green's displacements, stresses and stress derivatives for generally anisotropic solids developed by Tonon et al. (2001).

A circular tunnel 10 m in diameter is considered, and the BEM mesh is shown in Fig. 2. Infinite elements of the plane-strain type take into account the plane strain condition developing far away from the tunnel face (Beer and Watson, 1989). The tunnel axis is parallel to the x_2-axis (positive toward the North).

In order to cross-check the validity of Eqs. (1) and (2), and the BEM model, an isotropic rock mass was at first considered, with a Young's modulus of 5200 MPa

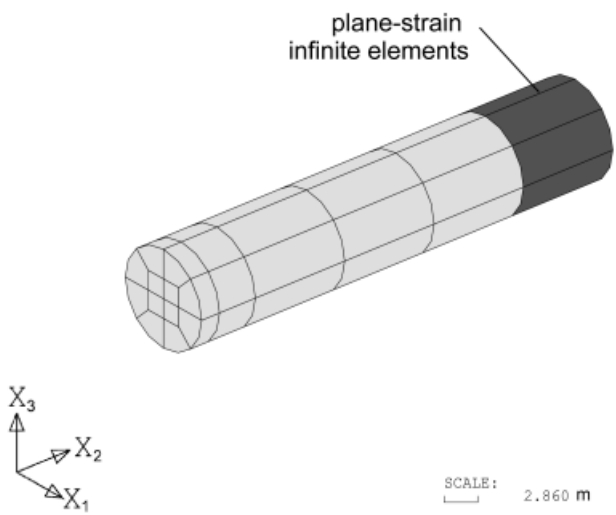

Fig. 2. BEM model of the tunnel (diameter $D = 10$ m); eight-node isoparametric boundary elements were used (in light gray)

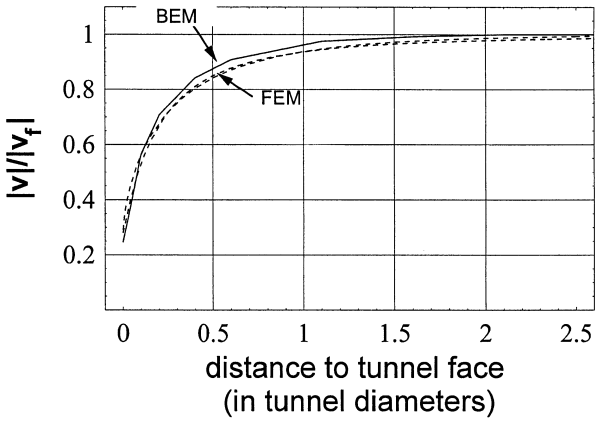

Fig. 3. Ratio between the magnitude of the displacement vector **v** and magnitude of the displacement vector far away from the tunnel face $\mathbf{v_f}$. Isotropic rock mass under a uniform state of stress. Comparison between displacements computed with the BEM model (continuous line) and those obtained with the closed-form solutions (dashed lines) proposed by Panet and Guenot (1982), and Corbetta et al. (1991) based on FEM computations

and a Poisson's ratio of 0.3; the state of stress is uniform and equal to 10 MPa. The results given in Fig. 3 show a good agreement between Eqs. (1) and (2), and the results predicted by the BEM model. We notice that Eqs. (1) and (2) are nearly indistinguishable, and slightly underestimate the displacements calculated by means of the BEM model. An explanation for this discrepancy may lie in the use of FEM models (notoriously stiffer than BEM models) used to derive Eqs. (1) and (2).

In the following examples, the rock mass is assumed to be transversely isotropic and to have the same (equivalent) elastic constants as the bedded sedimentary Waichecheng series described by Wittke (1990, pages 924–935). The following symbols and values have been used: E_1 = Young's modulus in the plane of transverse isotropy = 7800 MPa; E_2 = Young's modulus in direction perpendicular to the plane of transverse isotropy = 2400 MPa; v_1 = Poisson's ratio in planes parallel to the plane of transverse isotropy = 0.22; v_2 = Poisson's ratio in planes perpendicular to the plane of transverse isotropy = 0.07; G_2 = Shear modulus in plane perpendicular to the plane of transverse isotropy = 830 MPa.

The orientation of the plane of transverse isotropy is defined by the dip direction angle β and dip angle ψ, positive as shown in Fig. 4. In the following, (x_1, x_2, x_3) are three axes of global coordinates, whereas (y_1, y_2, y_3) are three axes of local coordinates attached to the plane of transverse isotropy as shown in Fig. 4. In particular, y_1 is parallel to the strike of the plane of transverse isotropy, and y_2 is parallel to the dip of the plane of transverse isotropy.

Because of the presence of an anisotropic rock mass, the displacements at the tunnel walls far from the tunnel face are, in general, no longer radial. The geomechanics convention for stresses is used (compressive stresses are positive).

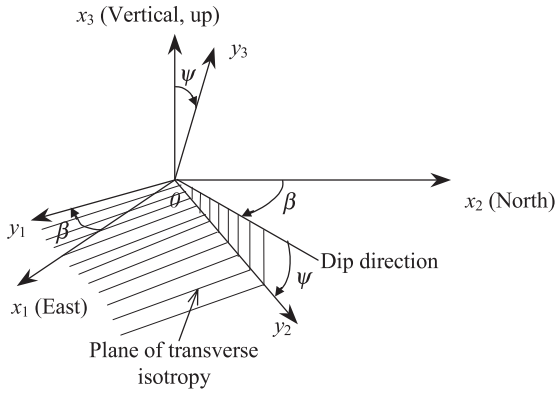

Fig. 4. Definition of the dip angle ψ and dip direction angle β

4. Plane of Transverse Isotropy Striking Parallel to the Tunnel Axis

4.1 Displacements Behind the Tunnel Face

The three spatial attitudes of the plane of transverse isotropy (referred to as cases *a*, *b*, and *c*) depicted in Figs. 5a–5c are considered. Two types of boundary conditions are applied: in Examples 1a, 1b, 1c, no lateral strain boundary conditions are applied with a vertical normal stress of 10 MPa, whereas in Examples 2a, 2b, 2c a uniform state of stress (10 MPa) is applied.

As shown by several authors (Wittke, 1990; Amadei et al., 1987; Amadei and Pan, 1992), under no lateral strain conditions, the *in situ* state of stress depends on the orientation of the plane of transverse isotropy, on the elastic properties of the rock mass, and on the vertical normal stress. Also, the strike direction of the plane of transverse isotropy, and the vertical direction are principal stress directions. Because x_2 is parallel to the strike direction (y_1-axis) of the plane of transverse isotropy, x_1, x_2, and x_3 are principal stress axes.

Table 1 summarizes the data for the examples studied. Points 1, 2, and 3 along the tunnel wall shown in Fig. 6 are monitored at different distances to the tunnel face.

The results of Examples 1.a to 1.c are given in Tables 2a to 2c, respectively, and, in dimensionless form, in Figures 7a to 7c. Only the displacement components in the x_1x_3 plane (plane orthogonal to the tunnel axis) have been analyzed. This is because the plane of transverse isotropy strikes parallel to the tunnel axis and thus the stress redistribution due to the excavation takes place under plane strain conditions far away from the tunnel face.

Because a uniform state of stress is assumed in Examples 2, only the results of Example 2.a are given in Table 2d and in Figure 7d. The results for Examples 2.b and 2.c are obtained by simply rotating the x_1x_3 axes by 90° or 45°, respectively, about the x_2 axis.

Figures 7a–7d show that, regardless of the anisotropy of the rock mass and of the boundary conditions, the displacements at Points 1 and 2 always follow

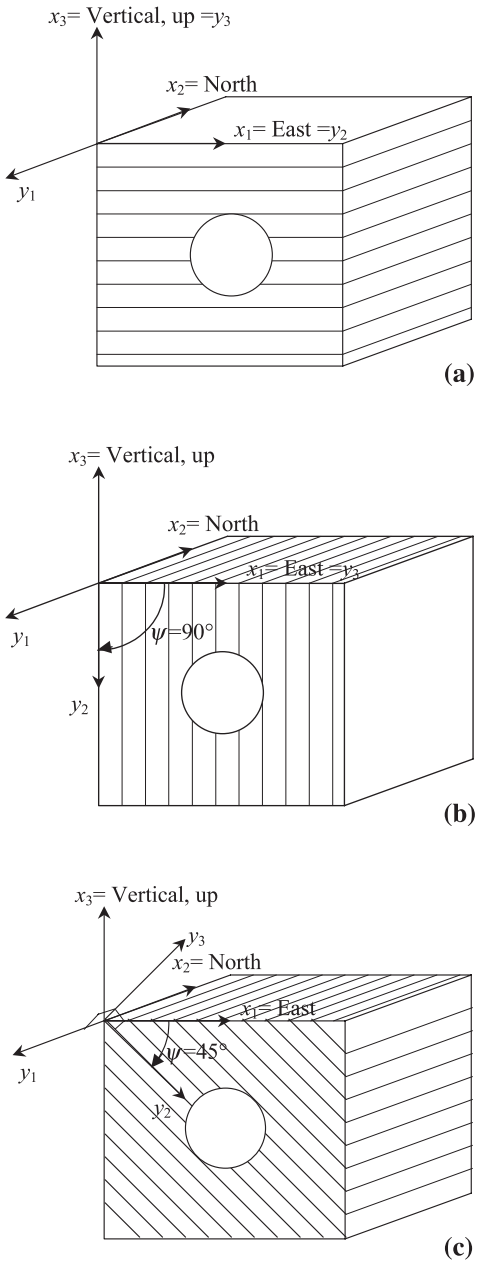

Fig. 5. Spatial orientation of the plane of transverse isotropy for Examples 1 and 2. (**a**) Case *a*: $\beta = 90°$, $\psi = 0°$; (**b**) Case *b*: $\beta = 90°$, $\psi = 90°$; (**c**) Case *c*: $\beta = 90°$, $\psi = 45°$

Table 1. *In situ* state of stress and orientation of the plane of transverse isotropy for the examples considered. In Examples 1, the x_1, x_2, x_3 axes are principal stress axes

Example	State of stress, MPa (referred to x_1, x_2, x_3 axes)	Dip direction/dip (β/ψ)
1.a	$\sigma_{11} = 2$; $\sigma_{22} = 2.9$; $\sigma_{33} = 10$	090/00
1.b	$\sigma_{11} = 0.87$; $\sigma_{22} = 2.4$; $\sigma_{33} = 10$	090/90
1.c	$\sigma_{11} = 4.47$; $\sigma_{22} = 3.24$; $\sigma_{33} = 10$	090/45
2.a	uniform; $p_0 = 10$	090/00
2.b	uniform; $p_0 = 10$	090/90
2.c	uniform; $p_0 = 10$	090/45

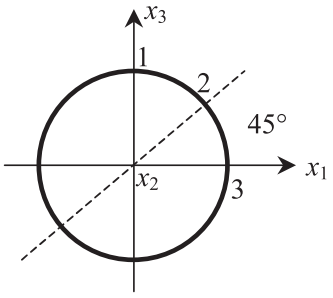

Fig. 6. Points 1, 2, and 3 monitored in Examples 1 and 2 (positive x_2-axis is orthogonal to the page and points into the page)

very closely Eqs. (1) and (2), which were derived for isotropic rock masses under a uniform state of stress. Point 3 is more sensitive to the anisotropy of the rock mass and to the boundary conditions. For Point 3, the largest deviation from the isotropic-uniform case is 40% (Example 1.a, Fig. 7a).

However, it must be noticed that the displacement magnitude at Point 3 is always smaller than the displacements at Points 1 and 2 by an order of magnitude (compare columns 6 and 7 with columns 2 and 3, and 4 and 5 in Tables 2). This is due either to the orientation of the plane of transverse isotropy (horizontal in Figs. 7a and 7d), or to the small *in situ* horizontal stress (Figures 7b and 7c). When these effects combine (Example 1.a, Fig. 7a), the deviation from the isotropic-uniform case is more evident.

When 2-D plane strain models of tunnels are used, it is necessary to calculate the fraction of displacement that takes place before the support/lining is installed. In this case, it is important to accurately estimate the displacements of the points which undergo the larger displacements, because these later points determine the support/lining loading. Errors of 40% in displacements that are an order of magnitude smaller do not introduce significant errors in the calculation of the rock mass-support/lining interaction.

In conclusion, Eqs. (1) and (2) can still be used when the rock mass is anisotropic and/or the *in situ* state of stress is not uniform. In other words, as the tunnel face advances, each point of the tunnel wall displaces by the same fraction, ξ_1, of

Table 2a. Example 1.a, displacements at points 1, 2, and 3 in Fig. 6 at distance d to the tunnel face

d (m)	Point 1		Point 2		Point 3	
	$-dx_1$ (m)	$-dx_3$ (m)	$-dx_1$ (m)	$-dx_3$ (m)	$-dx_1$ (m)	$-dx_3$ (m)
0	0	$0.112 \cdot 10^{-1}$	$0.758 \cdot 10^{-3}$	$0.804 \cdot 10^{-2}$	$0.742 \cdot 10^{-3}$	0
1	0	$0.209 \cdot 10^{-1}$	$0.709 \cdot 10^{-3}$	$0.151 \cdot 10^{-1}$	$0.845 \cdot 10^{-3}$	0
2	0	$0.252 \cdot 10^{-1}$	$0.693 \cdot 10^{-3}$	$0.181 \cdot 10^{-1}$	$0.911 \cdot 10^{-3}$	0
4	0	$0.297 \cdot 10^{-1}$	$0.872 \cdot 10^{-3}$	$0.211 \cdot 10^{-1}$	$0.122 \cdot 10^{-2}$	0
6	0	$0.321 \cdot 10^{-1}$	$0.106 \cdot 10^{-2}$	$0.228 \cdot 10^{-1}$	$0.148 \cdot 10^{-2}$	0
11	0	$0.349 \cdot 10^{-1}$	$0.143 \cdot 10^{-2}$	$0.247 \cdot 10^{-1}$	$0.201 \cdot 10^{-2}$	0
16	0	$0.360 \cdot 10^{-1}$	$0.167 \cdot 10^{-2}$	$0.254 \cdot 10^{-1}$	$0.233 \cdot 10^{-2}$	0
21	0	$0.365 \cdot 10^{-1}$	$0.180 \cdot 10^{-2}$	$0.259 \cdot 10^{-1}$	$0.254 \cdot 10^{-2}$	0
26	0	$0.368 \cdot 10^{-1}$	$0.189 \cdot 10^{-2}$	$0.260 \cdot 10^{-1}$	$0.265 \cdot 10^{-2}$	0

Table 2b. Example 1.b, displacements at points 1, 2, and 3 in Fig. 6 at distance d to the tunnel face

d (m)	Point 1		Point 2		Point 3	
	$-dx_1$ (m)	$-dx_3$ (m)	$-dx_1$ (m)	$-dx_3$ (m)	$-dx_1$ (m)	$-dx_3$ (m)
0	0	$0.520 \cdot 10^{-2}$	$0.126 \cdot 10^{-3}$	$0.376 \cdot 10^{-2}$	$0.162 \cdot 10^{-2}$	0
1	0	$0.952 \cdot 10^{-2}$	$0.143 \cdot 10^{-3}$	$0.707 \cdot 10^{-2}$	$0.190 \cdot 10^{-2}$	0
2	0	$0.119 \cdot 10^{-1}$	$0.156 \cdot 10^{-3}$	$0.873 \cdot 10^{-2}$	$0.228 \cdot 10^{-2}$	0
4	0	$0.145 \cdot 10^{-1}$	$0.197 \cdot 10^{-3}$	$0.106 \cdot 10^{-1}$	$0.293 \cdot 10^{-2}$	0
6	0	$0.162 \cdot 10^{-1}$	$0.234 \cdot 10^{-2}$	$0.117 \cdot 10^{-1}$	$0.345 \cdot 10^{-2}$	0
11	0	$0.185 \cdot 10^{-1}$	$0.302 \cdot 10^{-2}$	$0.131 \cdot 10^{-1}$	$0.433 \cdot 10^{-2}$	0
16	0	$0.195 \cdot 10^{-1}$	$0.341 \cdot 10^{-2}$	$0.138 \cdot 10^{-1}$	$0.486 \cdot 10^{-2}$	0
21	0	$0.201 \cdot 10^{-1}$	$0.364 \cdot 10^{-2}$	$0.142 \cdot 10^{-1}$	$0.515 \cdot 10^{-2}$	0
26	0	$0.203 \cdot 10^{-1}$	$0.376 \cdot 10^{-2}$	$0.144 \cdot 10^{-1}$	$0.534 \cdot 10^{-2}$	0

Table 2c. Example 1.c, displacements at points 1, 2, and 3 in Fig. 6 at distance d to the tunnel face

d (m)	Point 1		Point 2		Point 3	
	$-dx_1$ (m)	$-dx_3$ (m)	$-dx_1$ (m)	$-dx_3$ (m)	$-dx_1$ (m)	$-dx_3$ (m)
0	$0.314 \cdot 10^{-2}$	$0.810 \cdot 10^{-2}$	$0.253 \cdot 10^{-2}$	$0.693 \cdot 10^{-2}$	$0.761 \cdot 10^{-3}$	$0.156 \cdot 10^{-2}$
1	$0.605 \cdot 10^{-2}$	$0.150 \cdot 10^{-1}$	$0.592 \cdot 10^{-2}$	$0.127 \cdot 10^{-1}$	$0.302 \cdot 10^{-2}$	$0.279 \cdot 10^{-2}$
2	$0.707 \cdot 10^{-2}$	$0.181 \cdot 10^{-1}$	$0.734 \cdot 10^{-2}$	$0.151 \cdot 10^{-1}$	$0.385 \cdot 10^{-2}$	$0.322 \cdot 10^{-2}$
4	$0.808 \cdot 10^{-2}$	$0.213 \cdot 10^{-1}$	$0.862 \cdot 10^{-2}$	$0.177 \cdot 10^{-1}$	$0.448 \cdot 10^{-2}$	$0.365 \cdot 10^{-2}$
6	$0.856 \cdot 10^{-2}$	$0.230 \cdot 10^{-1}$	$0.920 \cdot 10^{-2}$	$0.190 \cdot 10^{-1}$	$0.470 \cdot 10^{-2}$	$0.384 \cdot 10^{-2}$
11	$0.898 \cdot 10^{-2}$	$0.250 \cdot 10^{-1}$	$0.966 \cdot 10^{-2}$	$0.205 \cdot 10^{-1}$	$0.483 \cdot 10^{-2}$	$0.406 \cdot 10^{-2}$
16	$0.910 \cdot 10^{-2}$	$0.258 \cdot 10^{-1}$	$0.975 \cdot 10^{-2}$	$0.211 \cdot 10^{-1}$	$0.473 \cdot 10^{-2}$	$0.405 \cdot 10^{-2}$
21	$0.913 \cdot 10^{-2}$	$0.262 \cdot 10^{-1}$	$0.975 \cdot 10^{-2}$	$0.214 \cdot 10^{-1}$	$0.411 \cdot 10^{-2}$	$0.472 \cdot 10^{-2}$
26	$0.915 \cdot 10^{-2}$	$0.264 \cdot 10^{-1}$	$0.973 \cdot 10^{-2}$	$0.215 \cdot 10^{-1}$	$0.406 \cdot 10^{-2}$	$0.463 \cdot 10^{-2}$

its final plane strain displacement. This fraction, ξ_1, is a function of the distance to the tunnel face and is well described by Eqs. (1) and (2).

To illustrate, let us suppose that a two stage 2-D plane strain model of a tunnel is available. In the first stage, the tunnel is excavated, and in the second stage the support/lining is installed. Because the rock mass is linearly elastic, the rock mass-

Table 2d. Example 2.a, displacements at points 1, 2, and 3 in Fig. 6 at distance d to the tunnel face

d (m)	Point 1		Point 2		Point 3	
	$-dx_1$ (m)	$-dx_3$ (m)	$-dx_1$ (m)	$-dx_3$ (m)	$-dx_1$ (m)	$-dx_3$ (m)
0	0	$0.863 \cdot 10^{-2}$	$0.156 \cdot 10^{-2}$	$0.615 \cdot 10^{-2}$	$0.218 \cdot 10^{-2}$	0
1	0	$0.177 \cdot 10^{-1}$	$0.407 \cdot 10^{-2}$	$0.128 \cdot 10^{-1}$	$0.556 \cdot 10^{-2}$	0
2	0	$0.216 \cdot 10^{-1}$	$0.538 \cdot 10^{-2}$	$0.155 \cdot 10^{-1}$	$0.731 \cdot 10^{-2}$	0
4	0	$0.255 \cdot 10^{-1}$	$0.662 \cdot 10^{-2}$	$0.182 \cdot 10^{-1}$	$0.907 \cdot 10^{-2}$	0
6	0	$0.274 \cdot 10^{-1}$	$0.730 \cdot 10^{-2}$	$0.195 \cdot 10^{-1}$	$0.101 \cdot 10^{-1}$	0
11	0	$0.294 \cdot 10^{-1}$	$0.809 \cdot 10^{-2}$	$0.209 \cdot 10^{-1}$	$0.114 \cdot 10^{-1}$	0
16	0	$0.301 \cdot 10^{-1}$	$0.842 \cdot 10^{-2}$	$0.213 \cdot 10^{-1}$	$0.119 \cdot 10^{-1}$	0
21	0	$0.304 \cdot 10^{-1}$	$0.857 \cdot 10^{-2}$	$0.215 \cdot 10^{-1}$	$0.121 \cdot 10^{-1}$	0
26	0	$0.305 \cdot 10^{-1}$	$0.865 \cdot 10^{-2}$	$0.216 \cdot 10^{-1}$	$0.122 \cdot 10^{-1}$	0

support/lining interaction is correctly taken into account if the portion of the *in situ* state of stress applied to the first stage is equal to (following Panet and Guenot, 1982):

$$\xi_1(d) = \left\{ 0.28 + 0.72 \cdot \left[1 - \left(\frac{1}{1 + \frac{d}{0.84R}} \right)^2 \right] \right\} \tag{3}$$

or, with very similar results (following Corbetta et al., 1991):

$$\xi_1(d) = \{0.29 + 0.71 \cdot [1 - e^{-1.5 \cdot (d/R)^{0.7}}]\}, \tag{4}$$

where:

d = distance to the tunnel face, R = tunnel radius.

In the case of Eq. (3), the portion of the *in situ* state of stress, ξ_2, to be applied to the second stage is equal to:

$$\xi_2(d) = 1 - \xi_1(d) = 1 - \left\{ 0.28 + 0.72 \cdot \left[1 - \left(\frac{1}{1 + \frac{d}{0.84R}} \right)^2 \right] \right\}. \tag{5}$$

or, in the case of Eq. (4):

$$\xi_2(d) = 1 - \xi_1(d) = 1 - \{0.29 + 0.71 \cdot [1 - e^{-1.5 \cdot (d/R)^{0.7}}]\}. \tag{6}$$

When the rock mass is anisotropic and/or the *in situ* state of stress is not uniform, the convergence curve (describing the radial displacement of the tunnel wall) and the confinement curve (describing the radial reaction of the support/lining) are not enough to solve the rock mass-support/lining interaction problem (see, for example, Hoek and Brown, 1980; Brady and Brown, 1993; Panet, 1995; Mammino and Tonon, 1997, for the classical convergence-confinement problem with only radial displacements). This is because the tunnel wall displacements have a radial

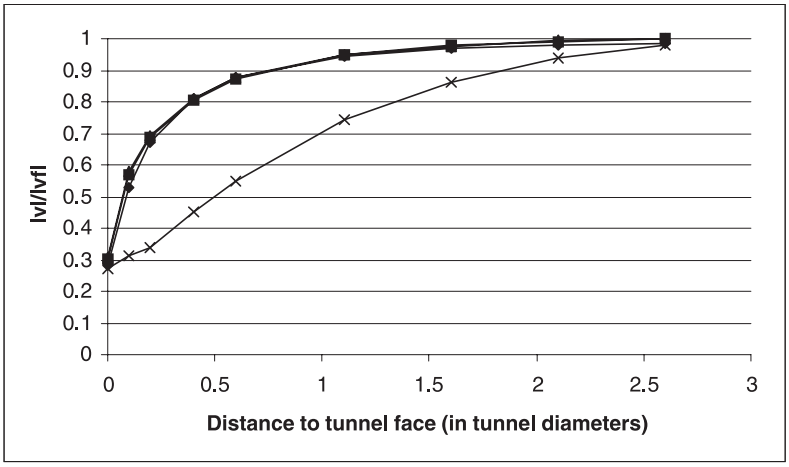

(a)

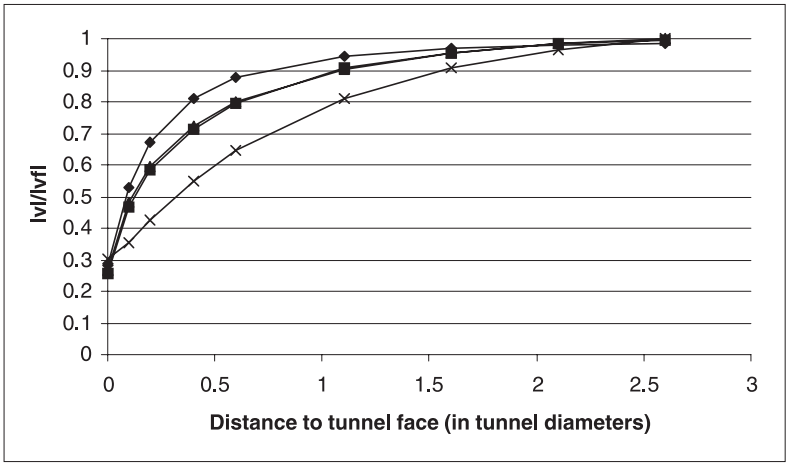

(b)

Fig. 7. (continued)

component as well as a tangential component, and the displacement magnitude (for a fixed distance to the tunnel face) varies along the tunnel wall. As a result, not only the radial, but also the flexural stiffness of the support/lining are called into play. The interaction problem can be easily dealt with numerically, as shown in the following Section.

4.2 Rock Mass-Shotcrete Interaction

Consider again Examples 1 and 2 described in Section 4.1 (Table 1). Here a 0.3-m thick shotcrete lining is applied 1 m behind the tunnel face. Young shotcrete displays a highly viscous behavior, which tends to reduce the stresses in the shot-

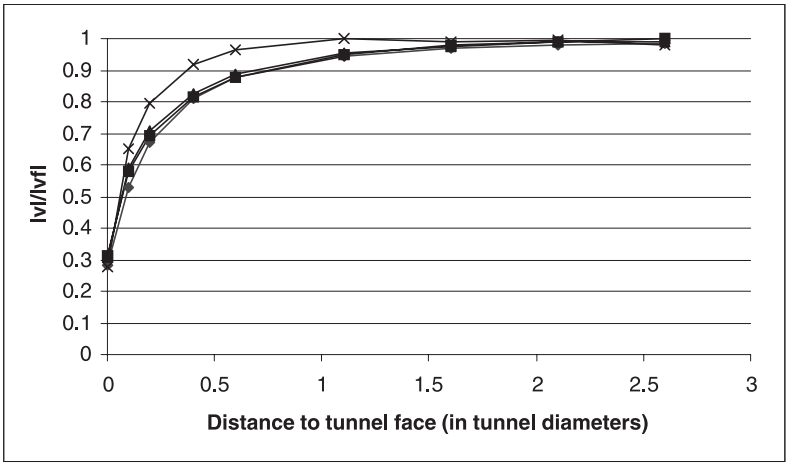

(c)

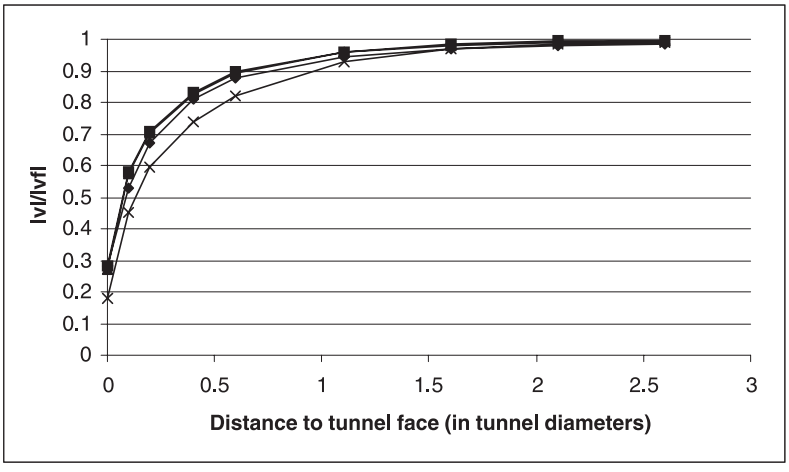

(d)

Fig. 7. Development of normalized tunnel wall displacements behind the tunnel face. —◆— Isotropic-uniform, —■— Point 1, —▲— Point 2, —x— Point 3. (**a**) Example 1.a (horizontal plane of transverse isotropy, no lateral strain boundary conditions); (**b**) Example 1.b (vertical plane of transverse isotropy, no lateral strain boundary conditions); (**c**) Example 1.c (inclined plane of transverse isotropy, no lateral strain boundary conditions); (**d**) Example 2.a (horizontal plane of transverse isotropy, uniform *in situ* state of stress). $\mathbf{v} = \sqrt{dx_1^2(d) + dx_3^2(d)}$; $\mathbf{vf} = \sqrt{dx_1^2(\infty) + dx_3^2(\infty)}$; dx_1 and dx_3 given in Tables 2a–2d

crete created by the interaction with the rock mass. In order to take into account this rheological property of the young shotcrete, Pottler (1990) showed that an equivalent linearly elastic behavior can be assumed for the shotcrete in two-dimensional ground-structure interaction calculations, provided a Young's modulus $E_c = 7$ GPa is used. A value $v_c = 0.2$ is assumed for the Poisson's ratio of the shotcrete.

A two-stage model is considered: in the first stage the tunnel is excavated, and in the second stage the lining is installed. According to Eqs. (3) and (4), the frac-

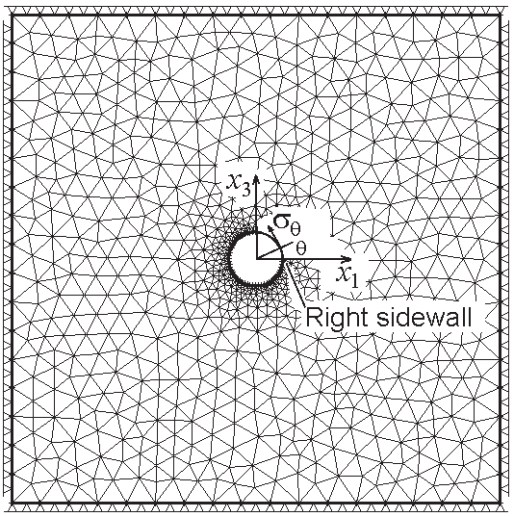

Fig. 8. 2-D plane strain FEM model; 6-node isoparametric triangular elements were used

tions ξ_1 of the *in situ* state of stress to be applied to the first stage (excavation only, without support) are 0.53 and 0.56, respectively. An average value of 0.545 will be used. The remaining 44.5% of the *in situ* state of stress is added during the second stage, after the lining has been installed (rock mass-lining interaction). A plane strain model of the tunnel was prepared using the 2-D Finite Element program Phase 2 Version 4.04 (Curran and Corkum, 1998). The mesh is shown in Fig. 8. The normal forces and the bending moments on the lining are summarized in Figs. 9 and 10, respectively.

In these figures, the solution for an isotropic rock mass in a uniform state of stress ($p_0 = 10$ MPa) is also shown. The Young's modulus considered is the harmonic average of E_1 and E_2 (Martino and Ribacchi, 1972):

$$\overline{E} = \left(\frac{1}{E_1} + \frac{1}{E_2}\right)^{-1} = 3670 \text{ MPa}.$$

The Poisson's ratio was assumed as: $v = v_1 = 0.22$.

This solution is calculated as follows. The radial stiffness of the shotcrete ring is (Mammino and Tonon, 1997, page 771):

$$k = \frac{E_c}{1 - v_c^2} \cdot \frac{s_c}{R} = 437.5 \text{ MPa},$$

where:

s_c = shotcrete thickness = 0.3 m, R = tunnel radius = 5 m.

The pressure exerted by the rock mass on the shotcrete ring (also equal to the pressure on the tunnel wall exerted by the lining) is (Mammino and Tonon,

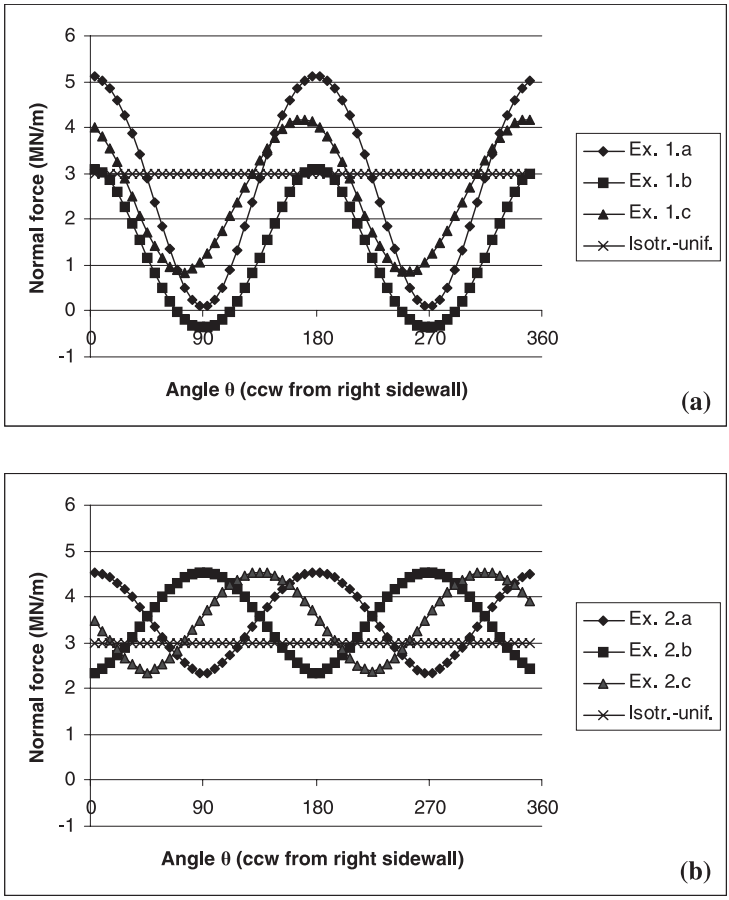

Fig. 9. Normal force (per unit length) in the shotcrete for Examples 1 and 2. (**a**) No lateral strain boundary conditions; (**b**) uniform *in situ* state of stress. Compressive forces are positive. Right sidewall has coordinates $(x_1, x_3) = (+5, 0)$, angle θ is defined in Fig. 8

1997, page 823):

$$p_i = 0.72 \cdot p_0 \cdot \frac{\left(\dfrac{1}{1 + \dfrac{d}{0.84 \cdot R}}\right)^2}{1 + \dfrac{E}{(1+\nu) \cdot k}} = 0.596 \text{ MPa},$$

where d is the distance to the tunnel face (1 m). The normal force (per unit length) is given by Mariotte's formula for thin tubes (Mammino and Tonon, 1997):

$$N = p_i R = 2.98 \text{ MN/m}.$$

Obviously, no bending moment arises in this case.

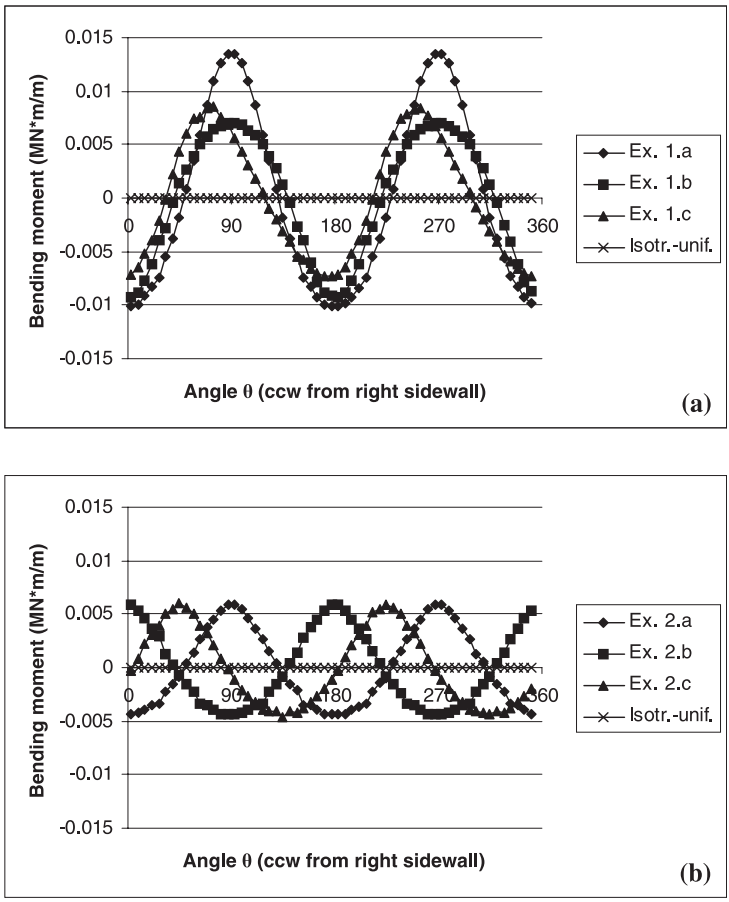

Fig. 10. Bending moment (per unit length) in the shotcrete for Examples 1 and 2. (**a**) no lateral strain boundary conditions; (**b**) uniform *in situ* state of stress. Positive bending moments stretch internal fibers. Right sidewall has coordinates $(x_1, x_3) = (+5, 0)$, angle θ is defined in Fig. 8

Upon examination of Figs. 9 and 10, the following can be noticed:

a) The maximum value of the normal force in the shotcrete is roughly the same for no lateral strain boundary conditions (Fig. 9a) and uniform *in situ* state of stress (Fig. 9b). On the other hand, the minimum normal force is very different for the two types of boundary conditions: negative (tensile) normal forces may develop in anisotropic rock masses under no lateral strain boundary conditions (Fig. 9a). The maximum fluctuations around the isotropic-uniform case are 50% (uniform *in situ* state of stress) and 110% (no lateral strain boundary conditions). In the presence of bending moments, a drastic reduction of the normal force may lead to failure of the shotcrete because large tensile stresses may develop; this is particularly important when the minimum values of the normal

forces (Fig. 9a) correspond to maximum values of the bending moments (Fig. 10a).

b) As for the bending moments, the oscillation around the isotropic-uniform case (zero bending moment) is 2 to 3 times larger in the no lateral strain boundary condition hypothesis than in the uniform state of stress hypothesis.

c) If the effects of elastic anisotropy only (uniform *in situ* state of stress) are absorbed by the factors of safety usually adopted, the combined effects of elastic anisotropy and no lateral strain boundary conditions lead to failure of the shotcrete if the shotcrete is designed for an isotropic rock mass under a uniform state of stress. This conclusion emphasizes the importance of a correct estimation of the boundary conditions (Tonon et al., 2001).

5. Plane of Transverse Isotropy not Striking Parallel to the Tunnel Axis

In the following examples, the tunnel wall displacements are fully three-dimensional, thus it is necessary to plot the displacement magnitudes, for useful comparison. Also, the displacements change from point to point along a cross section of the tunnel wall. We will restrict ourselves to the crown displacements.

Examples 3 and 4 are aimed at assessing the effect of the inclination of the plane of transverse isotropy with respect to the tunnel. In both cases, the strike of the plane of transverse isotropy is orthogonal to the tunnel axis. In Example 3, the tunnel is excavated "with dip" (Fig. 11a), $\beta = 180°$, $\psi = 45°$, whereas in Example 4 the excavation proceeds "against dip" (Fig. 11b), $\beta = 0°$, $\psi = 45°$. The pre-mining state of stress is uniform (10 MPa).

The results, displayed in Figure 11c, clearly indicate that, when the tunnel is driven with dip, over 60% of the total displacement has already occurred at the tunnel face; as a consequence, Eqs. (1) and (2) largely underestimate the initial displacements. Hence, if Eqs. (1) and (2) are used to calculate the initial convergence for a 2-D model, the calculated displacements and stresses of the reinforcement/lining at the crown are considerably overestimated.

The converse is true if the tunnel is excavated against dip. Less than 10% of the total displacement has occurred at the tunnel face: as a consequence, Eqs. (1) and (2) largely overestimate the initial displacements. So, if Eqs. (1) and (2) are used to calculate the initial convergence for a 2-D model, the calculated displacements and stresses of the reinforcement/lining at the crown are considerably underestimated.

In general, for a given transversely isotropic rock mass whose plane of transverse isotropy is not parallel to the tunnel axis, the reinforcement/lining at the crown will be more strained when mining against dip. Thus it is easier to control the tunnel wall deformation at the crown when tunneling against dip.

An explanation of this phenomenon may be as follows. A transversely isotropic rock mass is stiffer in direction parallel to the plane of isotropy and more deformable in direction normal to it. When excavating with dip, the rock mass at the crown is more deformable toward the excavated part of the tunnel. Thus the rock mass can freely expand toward the inside of the tunnel (zone A in Fig. 11a). This is evident in Fig. 12a, showing the displacements at the face (vector a), at 0.1

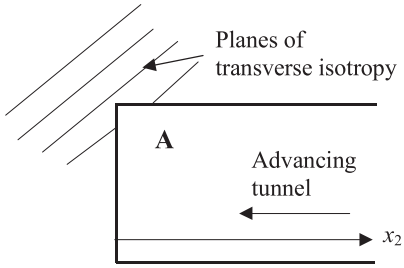

(a)

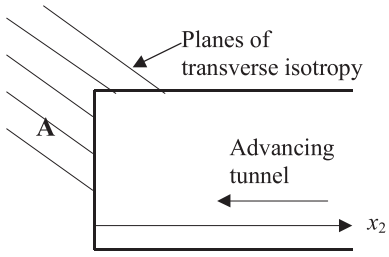

(b)

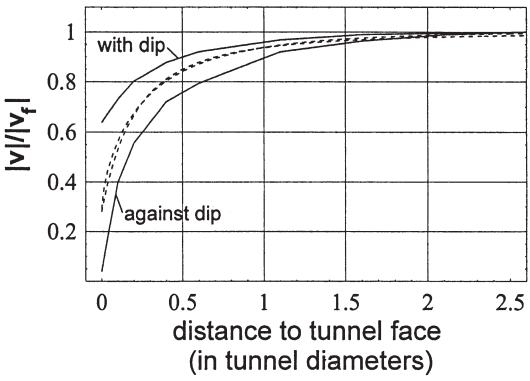

(c)

Fig. 11. (**a**) Tunneling with dip; (**b**) tunneling against dip; (**c**) ratio between magnitude of the displacement vector **v** and magnitude of the displacement vector far away from the tunnel face $\mathbf{v_f}$. The dashed lines refer to the closed-form solutions for isotropic rock mass in a uniform state of stress (Eqs. 1 and 2)

diameters to the face (vector b), and at 2 diameters to the face (vector c): all the displacements point toward the inside of the excavated tunnel, so the crown is free to move toward its final position in the empty space of the tunnel, and thus the displacement magnitude is very large since the beginning (vector a). On the contrary, when excavating against dip, the rock mass is more deformable toward the non-excavated part of the tunnel. Thus, the rock mass at the crown cannot freely

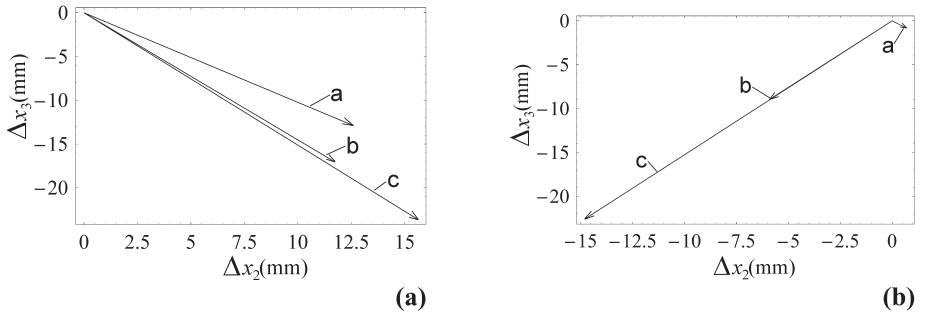

Fig. 12. Examples 3 and 4. Displacements at the tunnel face (vector a), at 0.1 diameters to the tunnel face (vector b), at 2 diameters to the tunnel face (vector c). (**a**) tunneling with dip; (**b**) tunneling against dip. Axis x_2 is positive toward the excavated part of the tunnel, axis x_3 is positive upwards (see Figs. 2 and 4). Because the pre-mining state of stress is uniform and the plane of transverse isotropy strikes orthogonal to the tunnel axis, the displacement vectors have no component along the x_1-axis

expand toward its final position because of the presence of the core of rock still to be excavated (zone A in Fig. 11b). As can be seen in Fig. 12b, the crown has eventually to displace toward the non yet excavated part of the tunnel (vector c), but it cannot do so at the face, because of the presence of the rock still to be excavated. In fact, the initial displacement points toward the excavated tunnel (the only kinematically permissible direction), even if the displacement magnitude is very small. When the tunnel face advances, the wall can finally move toward the face (vectors b, c).

The different behavior of the crown displacements also affects the state of stress in the shotcrete lining applied to the tunnel walls. As can be seen in Fig. 12a, when driving with dip, the component along the x_2-axis increases, thus a shotcrete layer installed close to the face will be pushed toward the existing shotcrete, as the face advances. This causes longitudinal compression in the concrete. In order to get an order of magnitude, consider a shotcrete applied at the face and assume that the three-dimensional dome effect of the tunnel face takes place over two diameters behind the face. In the case of Fig. 12a (driving with dip), the final strain in the tunnel axis direction is (only the difference between the x_2-component of the *c* and the *a* vectors contributes to the shotcrete longitudinal strain):

$$\varepsilon_{22} = \frac{(15 - 12.5) \cdot 10^{-3}}{2 \cdot 10} = 5 \cdot 10^{-5}. \tag{7}$$

If a Young's modulus of 7000 MPa is adopted for the shotcrete (Pottler, 1990), the longitudinal stress is:

$$\sigma_{22} = 5 \cdot 10^{-5} \cdot 7000 = 0.35 \text{ MPa (compressive)} \tag{8}$$

which is not very substantial and causes no problem to the shotcrete.

When driving against dip (Fig. 12b) the x_2-component of the displacement decreases and thus the new layer of shotcrete is pulled by the rock mass away from the existing shotcrete. As an upper bound, we can proceed as in Eqs. (7) and (8).

Table 3. Orientation of the plane of transverse isotropy and *in situ* state of stress for the examples considered

Example	Plane of transverse isotropy Dipdir/dip = β/ψ	*In situ* state of stress
5	045/45	uniform (10 MPa)
6	060/60	uniform (10 MPa)
7	000/45	non-uniform
8	045/45	non-uniform
9	060/60	non-uniform

The final strain is:

$$\varepsilon_{22} = \frac{-15 \cdot 10^{-3}}{2 \cdot 10} = -7.5 \cdot 10^{-4}, \tag{9}$$

which is of the same order of magnitude of concrete shrinkage. The corresponding longitudinal stress is:

$$\sigma_{22} = -7.5 \cdot 10^{-4} \cdot 7000 = -5.25 \text{ MPa (tensile)}. \tag{10}$$

This can be a substantial value for a young concrete, and can lead to circumferential cracking.

Next, we study the effect of slight changes in the dip direction and dip of the plane of transverse isotropy with respect to the "driving with dip" case (Example 3). Also, the effect of a non-uniform state of stress is studied (see Table 3). More specifically, Examples 5 and 6 have a uniform *in situ* state of stress (10 MPa), and perturbed orientation of the plane of transverse isotropy. Examples 7, 8, 9 have the same orientation of the plane of transverse isotropy as in Examples 3, 4, and 5, respectively, but the pre-mining state of stress is not uniform. The principal stresses are: $\sigma_1 = 16.0$ MPa, $\sigma_2 = 9.2$ MPa, $\sigma_3 = 1.7$ MPa. Their orientations are given by the following unit eigenvectors (components with respect to the x_1, x_2, x_3 axes in Figs. 2 and 4): $\mathbf{w}_1 = (-0.396, -0.233, 0.888)$; $\mathbf{w}_2 = (0.518, -0.855, 0.007)$; $\mathbf{w}_3 = (0.758, 0.463, 0.460)$. Table 3 summarizes the examples considered.

The results are shown in Fig. 13. It turns out that the trend seen before (Example 3, Fig. 11c) is respected, regardless of the state of stress and even if the strike of the plane of transverse isotropy is not orthogonal to the tunnel axis, or the dip is different from 45°.

In conclusion, when the plane of transverse isotropy is not parallel to the tunnel axis, the amount of displacement behind the tunnel face cannot be estimated by means of formulas valid for isotropic media (Eqs. 1 and 2). Three-dimensional models are necessary in this case.

6. Conclusions

The effect of elastic anisotropy (transverse isotropy) on the convergence behind a tunnel face has been investigated by means of a parametric study. Two cases are distinguished, according to whether the plane of transverse isotropy strikes parallel to the tunnel axis or not.

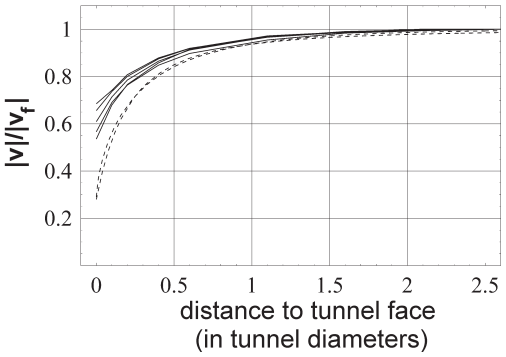

Fig. 13. Ratio between magnitude of the displacement vector **v** and magnitude of the displacement vector far away from the tunnel face $\mathbf{v_f}$. Continuous lines refer to tunneling with dip (Examples 5–9 in Table 3). The dashed lines refer to the closed-form solutions for an isotropic rock mass under a uniform *in situ* state of stress (Eqs. 1 and 2)

When the plane of transverse isotropy strikes parallel to the tunnel axis, as the tunnel face advances, each point of the tunnel wall displaces by the same fraction of its final plane strain displacement. This fraction is a function of the distance to the tunnel face, and is well described by the usual expressions valid for isotropic rock masses under a uniform state of stress. Thus, two-dimensional analyses of rock mass-structure interaction can be performed.

Two-dimensional analyses show that if the effects of elastic anisotropy only are absorbed by the factors of safety usually adopted, the combined effects of elastic anisotropy and no lateral strain boundary conditions lead to failure of the shotcrete if the later is designed for an isotropic rock mass under a uniform state of stress.

When the plane of transverse isotropy does not strike parallel to the tunnel axis, the usual expressions valid for isotropic rock masses under a uniform state of stress are not applicable. Thus, two-dimensional analyses of rock mass-structure interaction cannot be performed, and three-dimensional analyses are necessary.

Acknowledgements

This research is funded by National Science Foundation under grant no. CMS-9713559. The authors would like to thank Prof. Beer, Mr. Duenser and Mr. Golser (Technical University of Graz, Austria) for their technical support while using BEFE. Program BEFE has been used according to contract between CSS (Graz, Austria) and the University of Colorado at Boulder (USA).

The valuable comments of the anonymous reviewers and of the co-editor Prof. Einstein are greatly appreciated.

References

Amadei, B., Pan, E. (1992): Gravitational stresses in anisotropic rock masses with inclined strata. Int. J. Rock Mech. Min. Sci. Geomech. Abstr. 29 (3), 225–236.

Amadei, B., Savage, W. Z., Swolfs, H. S. (1987): Gravitational stress in anisotropic rock masses. Int. J. Rock Mech. Min. Sci. Geomech. Abstr. 24 (1), 5–14.

Beer, G. (1999): BEFE User's Manual. CSS, Graz, Austria.

Beer, G., Watson, J. O. (1989): Infinite boundary elements. Int. J. Numer. Meth. Eng. 28, 1233–1247.

Bernaud, D., Rousset, G. (1992): La "Nouvelle Méthode Implicite" pour l'étude du dimensionnement des tunnels. Rev. Franç. Géotech. 60, 5–26.

Bernaud, D., Rousset, G. (1996): The new implicit method for tunnel analysis (short communication). Int. J. Numer. Anal. Meth. Geomech. 20, 673–690.

Brady, B. H. G., Brown, E. T. (1993): Rock mechanics for underground mining, 2nd edn. Chapman & Hall, London.

Corbetta, F., Bernaud, D., Nguyen-Mihn, D. (1991): Contribution à la méthode convergence-confinement par le principe de la similitude. Rev. Franç. Géotech. 54, 5–11.

Curran, J. H., Corkum, B. T. (1998): Phase 2. 2D finite element program for calculating stresses and estimating support around underground excavations. Reference Manual and Tutorial Manual. Rockscience, Toronto.

Hoek, E., Brown, E. T. (1980): Underground excavations in rock. Institution of Mining and Metallurgy, London, UK.

Mammino, A., Tonon, F. (1997): Opere strutturali per l'ingegneria territoriale, vol. 1, Tome 2. Alinea Editrice, Firenze.

Martino, D., Ribacchi, R. (1972): Osservazioni su alcuni metodi di misura delle caratteristiche elastiche di rocce o ammassi rocciosi, con particolare riferimento al problema dell'anisotropia. L'Industria Mineraria, Serie II, XXIII (5), 193–203.

Nguyen-Minh, D., Guo, C. (1993): A ground-support interaction principle for constant rate advancing tunnels. In: Proc., EUROCK '93, Lisboa, Portugal, Balkema, Rotterdam, 171–177.

Nguyen-Minh, D., Guo, C. (1996): Recent progress in Convergence-Confinement method. In: Barla, G. (ed.), Proc., EUROCK '96, vol. 2. A.A. Balkema, Rotterdam, 855–860.

Panet, M. (1995): Calcul des tunnels par la méthode convergence-confinement. Presses de l'Ecole Nationale de Ponts et Chaussés, France.

Panet, M., Guenot, A. (1982): Analysis of convergence behind the face of a tunnel. In: Tunnelling '82. The Institution of Mining and Metallurgy, London, 197–204.

Pottler, R. (1990): Time-dependent rock-shotcrete interaction. A numerical shortcut. Comput. Geotech. 9, 29–49.

Tonon, F., Pan, E., Amadei, B. (2001): Green's functions and BEM formulation in general anisotropic elastic solids. Comput. Struct. 79 (5), 469–482.

Tonon, F., Amadei, B., Pan, E. (2001) Bayesian estimation of boundary conditions with application to deep tunneling. Geotech. Geol. Engng. 19, 43–67.

Wittke, W. (1990): Rock mechanics. Springer, Berlin Heidelberg New York Tokyo. (English translation of Wittke, 1984, Felsmechanik. Springer, Berlin Heidelberg New York Tokyo).

Authors' address: Dr. Fulvio Tonon, Vicolo S. Antonino A, 3, I-31100 Treviso, Italy. E-mail: tonon@geophys.utah.edu